

Electronic and crystal structure of Cu_{2-x}S : Full-potential electronic structure calculations

Pavel Lukashev* and Walter R. L. Lambrecht

Department of Physics, Case Western Reserve University, Cleveland, Ohio 44106-7079, USA

Takao Kotani and Mark van Schilfgaarde

School of Materials, Arizona State University, Tempe, Arizona 85287, USA

(Received 9 July 2007; published 2 November 2007)

Electronic structure calculations are presented for Cu_{2-x}S using the full-potential linearized muffin-tin orbital method. In the simple cubic antiferroite structure, Cu_2S is found to be semimetallic both in the local density approximation (LDA) and using the quasiparticle self-consistent *GW* (QSGW) method. This is because the Cu *d* bands comprising the valence band maximum are degenerate at the Γ point and the fact that the Cu *s* band, which can be considered to be the lowest conduction band, lies slightly below it at Γ . Small deviations from the ideal antiferroite positions for the Cu atoms, however, open a small gap between the Cu *d* valence and Cu *s*-like conduction bands because the symmetry breaking allows the Cu *s* and Cu *d* bands to hybridize. Supercell models are constructed for cubic and hexagonal chalcocite Cu_2S as well as cubic digenite $\text{Cu}_{1.8}\text{S}$ by means of a weighted random number structure generating algorithm. This approach generates models with Wyckoff site occupancies adjusted to those obtained from experimental x-ray diffraction results and with the constraint that atoms should stay within reasonable distance from each other. The band structures of these models as well as of the low-chalcocite monoclinic structure ($\text{Cu}_{0.6}\text{S}_{0.4}$) are calculated in LDA with an additional Cu *s* shift obtained from the QSGW-LDA difference for the antiferroite structure. Even with this correction, smaller band gaps of about 0.4–0.6 eV (increasing from cubic to hexagonal to monoclinic) than experimentally observed (1.1–1.2 eV) are obtained for the Cu_2S composition. Decreasing the Cu content of Cu_{2-x}S in the range $0.06 < x < 0.2$ is found to essentially dope the *p*-type material by placing the Fermi level 0.2–0.3 eV below the valence band maximum but also to increase the gap between highest partially filled valence band and lowest conduction bands to about 0.7–1.0 eV. This results from a reduced Cu *d*-band width. Thus, the optical band gap or onset of optical absorption increases in part but not exclusively due to the Moss-Burstein effect. The total energies of the structures are found to increase from monoclinic to hexagonal to cubic to antiferroite. This is consistent with the fact that the simple antiferroite structure is not observed and that the systems change from monoclinic to hexagonal to cubic with increasing temperature, under the assumption that the electronic energy of the system dominates the free energy. We find that Cu_2S is unstable toward the formation of Cu vacancies even in thermodynamic equilibrium with bulk Cu metal. The experimental data on the band gaps and optical absorption are discussed. We find no evidence for indirect band gaps in the hexagonal materials and argue that the experimental results are consistent with this in spite of previous reports to the contrary. The presence of a second onset of absorption located about 0.5 eV higher than the minimum band gap observed in experiment is explained by a rise in conduction band density of states at this energy in our calculations. The calculated increase in gap with decreasing Cu concentration is in agreement with experimental observations.

DOI: [10.1103/PhysRevB.76.195202](https://doi.org/10.1103/PhysRevB.76.195202)

PACS number(s): 71.23.-k, 71.20.Nr, 72.40.+w, 73.22.-f

I. INTRODUCTION

Copper sulfides, in particular, Cu_{2-x}S , were used in some of the earliest thin-film solar cells.^{1,2} The earliest report mentions an unusually high photovoltaic effect in CdS, which was possibly due to Cu from the contacts diffusing into the CdS.³ It is naturally a *p*-type semiconductor (due to slight nonstoichiometry with less than two Cu atoms per S) and was used in conjunction with *n*-type CdS.⁴ In fact, Cu_2S in these early solar cells was prepared by Cu infiltrating the CdS lattice and replacing Cd atoms.^{5,6} While solar cells with efficiencies up to 9% were achieved,¹ the solar cells suffered from long-time deterioration in air⁷ and further development of them was mostly stopped.⁶ Recently, a renewed interest in Cu_2S has occurred because now Cu_2S can be grown in nanoparticle form,^{8–11} and this opens the way to new potential applications, including new approaches to photovoltaics.^{12–15}

In spite of this rather long-standing interest in Cu_2S , very little is definitely known about its electronic structure. In particular, there have not been any computational investigations, to the best of our knowledge. So, all we know about the band structure are the gaps obtained from optical absorption measurements^{7,16–18} and photoconductivity.¹⁹ Different indirect gap schemes were proposed based on the optical data but were never confirmed by calculations. The main reason for this is no doubt the complex crystal structure. In the crystallography literature, elucidating the structure of the various mineral forms of Cu_{2-x}S has been a long-standing and challenging problem.^{20–28} The main reason for this is that the positions of the Cu atoms within the close-packed sublattice of S atoms are not well defined. They depend on temperature and, at elevated temperatures the Cu atoms, are, in fact, unusually mobile, thus making Cu_2S a partially ionic conductor.²⁹ Under these circumstances, crystallographers

can only determine a statistical distribution of Cu atoms.

This unusually mobile behavior of the Cu atoms is interesting in its own right but it also presents a challenge in computation of the electronic structure. It could possibly lead to strong phonon scattering and electron-phonon interactions. The strong phonon scattering coupled with relatively high conductivity could be interesting for thermoelectric properties, although this has not yet been pursued. At present, it seems mostly a problem, because it can easily lead to deterioration by Cu leaking out of the material and changes in stoichiometry over time.

In this paper, we first consider a simplified crystal structure with high symmetry, namely, the antiferroite structure. To our surprise, the electronic structure in this case turned out to be semimetallic. Band gaps are usually underestimated by the local density approximation. The metallic band structure, however, is confirmed by a recently developed “quasiparticle self-consistent *GW*” (QSGW) method.^{30–34} A comparison of the QSGW with local density approximation (LDA) results and analysis of the atomic orbital character of the bands provide important insights in the electronic structure. In particular, it shows that the Cu *s* orbitals need to be shifted slightly upward.

In the next step, we describe a method for generating model crystal structures using a weighted random number generator. The resulting models are shown to represent the experimental statistical distribution of the Cu atoms quite well. However, they require fairly large structural models for which, unfortunately, we cannot yet apply the QSGW approach. The LDA band-structure calculations show that the complexity of the crystal structure is essential to open a band gap. However, the band gap is much smaller than the experimentally reported values. Applying the insights of the combined LDA-QSGW study of the simpler antiferroite structure, we then attempt to correct the band gaps by including semi-empirical shifts of the relevant Cu *s* states. We also discuss the effects of nonstoichiometry, i.e., a lower Cu concentration, and estimate effective masses. We provide a critical examination of the experimental data in comparison with our calculated results, including some results on recent nanoparticles. This shows that our calculations still underestimate the band gaps by about 0.6 eV, but nevertheless, significant information on the nature of the band structure is obtained from our calculations. For example, our calculations allow us to clarify the band gaps to be direct rather than indirect. They explain the occurrence of a second onset in the optical absorption at about 0.5 eV above the gap and explain the increase in gap with decreasing Cu content. Our analysis of the total energies also shows the intrinsic instability of Cu₂S toward Cu-vacancy formation.

The paper is organized as follows. In Sec. II, we describe the computational approach. In Sec. III, we summarize what is known about the crystal structure from the literature and review the nomenclature of the various mineral forms. Section IV is divided in sections on the simple antiferroite structure (Sec. IV A), the derivation of our model structures (Sec. IV B), and the band-structure results for the model structures (Sec. IV C). Finally, in Sec. IV D, we comment on the relative total energies of the various models we have studied. In Sec. V, we critically review the experimental data on optical

absorption in comparison with our calculated results. A summary of the main results concludes the paper (Sec. VI).

II. COMPUTATIONAL METHODS

The main ingredients of our computational method are the density functional theory³⁵ in the local density approximation (LDA),³⁶ the full-potential linearized muffin-tin orbital method (FP-LMTO),^{37,38} and a recently developed form of the *GW* method,^{39,40} called the quasiparticle self-consistent *GW* (QSGW).^{30–34}

The FP-LMTO uses a basis set of augmented smoothed Hankel functions.³⁸ This allows one to fine tune the shape of the orbital both inside the muffin-tin sphere and outside it so that a fairly small accurate basis set of only two sets *s, p, d* and *s, p* orbitals per atom can be used, thus allowing us to easily treat large unit cells. The basis set can be augmented with extra orbitals per *l* channel and higher *l* values when necessary for higher accuracy. For example, for the QSGW calculations, a basis set including *f* orbitals and a second set of *s-d* were employed. The potential is free of shape approximations, and the smooth parts of the charge density, potential, and wave functions are tabulated on a real space mesh. The Brillouin-zone integrations were carried out using a regularly spaced mesh with a mesh size adapted according to cell size. For instance, for the simple antiferroite structure, the reciprocal unit cell is divided into 6 in each direction, while for the largest cells, a division into 2 or even 1 is already found to be sufficient.

The one-electron eigenvalues in density functional theory, in particular, in the local density approximation, are not reliable to predict one-electron excitations, i.e., the band structure, and, as a result, typically underestimate band gaps of semiconductors severely. This is because the theory is designed to describe the total energies of the ground state only. A better theory for one-electron excitations is provided by Hedin’s *GW* method.³⁹ In this approach, the quasiparticle excitation energies E_i are obtained from

$$\left[-\frac{1}{2}\nabla^2 + v_H(\mathbf{r}) \right] \psi_i(\mathbf{r}) + \int \Sigma(\mathbf{r}, \mathbf{r}', E_i) \psi_i(\mathbf{r}') d^3 r' = E_i \psi_i(\mathbf{r}), \quad (1)$$

in which atomic Hartree units are used, v_H is the Hartree potential, and $\Sigma(\mathbf{r}, \mathbf{r}', E)$ is a nonlocal and energy dependent self-energy operator. In the *GW* approximation, Σ is obtained from the one-electron Green’s function G and the screened Coulomb interaction W ; hence, the name *GW*. More precisely, $\Sigma(\mathbf{r}, \mathbf{r}', E)$ is the time to energy Fourier transform of $\Sigma(12) = iG(12)W(1+2)$, in which 1 and 2 stand for the position (plus, if necessary, spin) and time of particles 1 and 2. The dynamically screened Coulomb interaction $W(12) = v(12) + \int W(13)\Pi(34)v(42)d34$ involves the polarizability Π , which, in the random phase approximation (RPA), is given by $\Pi(1, 2) = -iG(1, 2)G(2, 1)$. Since Π is determined through G , so is W . Therefore, Σ may be viewed as a functional of G .^{39,40}

The calculations here, at least for the simplest possible structure, are carried out using the QSGW approx-

imation.^{32,34} Because it is new, we briefly describe its main ideas. Hedin's *GW* approximation is almost invariably implemented with further approximations made. The most important among these are the pseudopotential approximation (which treats the core with LDA and then pseudizing it) and the lack of self-consistency (*G* and *W* are generated from LDA eigenfunctions and eigenvalues, i.e., $G^{\text{LDA}}W^{\text{LDA}}$). Because *GW* is a perturbation theory, the results clearly depend on the starting point. Thus, the errors in energy bands can originate from (i) the validity of the RPA approximation to Π and (ii) the validity of the *GW* approximation to Σ . The size of both of these errors depends on (iii) the starting Green's function *G* and, finally, (iv) further simplifications to an exact implementation of the *GW* approximation. These further approximations (iv) have plagued the *GW* community because calculated results of the same quantities tend to vary between different groups, much as what occurred in the early days of the LDA. However, the most recent all-electron implementations of *GW* such as the method used in the present work³⁰⁻³⁴ largely eliminate these errors. However, in recent years, it has been recognized that (iii) is also critical; CuBr is an important example of this.³³ One may thus also expect it to be important for the present case of Cu₂S.

QSGW is a prescription to minimize errors (i) and (ii) through an optimal choice of (iii) within the *GW* framework. A self-consistency condition is especially constructed so as to bring the Green's function *G* around which the perturbation theory is done as close as possible to the exact *G*, so as to minimize the size of the perturbation. More specifically, the exchange-correlation potential of the unperturbed Hamiltonian is chosen to be

$$V_{xc} = \frac{1}{2} \sum_{ij} |\psi_i\rangle \{ \text{Re} \Sigma(\epsilon_i)_{ij} + \text{Re} \Sigma(\epsilon_j)_{ij} \} \langle \psi_j|, \quad (2)$$

where Re indicates that only the Hermitian part is taken and ϵ_i are the eigenvalues of the unperturbed Hamiltonian. Thus, the effective potential in the starting one-particle Hamiltonian, which determines *G* and Π , is itself determined by Σ , and this provides another self-consistency requirement. For a full discussion of the justifications of this approach, we refer the reader to Ref. 34.

With an all-electron implementation of *GW* and the self-consistency condition, energy bands are predicted with uniformly good accuracy for a wide range of semiconductors; moreover, the errors remaining are highly systematic.^{32,34} Self-consistency improves agreement with experiment and is sometimes essential: the band gap of CuBr, for example, is 1.56 eV in the $G^{\text{LDA}}W^{\text{LDA}}$ approximation,³³ far below the observed fundamental gap of ~ 3.1 eV. Self-consistency brings the gap to within ~ 0.2 eV of experiment, not only for CuBr but also for a wide range of semiconductors.³² Detailed discussions of standard LDA-based *GW* and QSGW can be found in Refs. 33 and 34.

QSGW overestimates semiconductor band gaps slightly. A key point that distinguishes QSGW from all other approaches is that the error is highly systematic. Most of the error can be qualitatively understood from the omission of excitonic effects in the calculation of Π . In any case, we can reasonably

expect that QSGW calculations predict energy bands of Cu₂S and CuBr accurate to ~ 0.2 eV for a given crystal structure.

Since QSGW is too expensive for the rather complicated structures we study here, we used QSGW only for the simple cubic antiferroite structure. We adopt the LDA but adjust the LDA potential to approximately match QSGW bands of bulk Cu₂S in this particular structure and then use the same potential for the more realistic structures. From the analysis of the QSGW compared to the LDA results, we learn that primarily, the Cu *s* orbital energy needs to be shifted upward. In the FP-LMTO method, this can be done by adding a projector operator to the Hamiltonian,

$$V_s = |\phi_s\rangle \Delta_s \langle \phi_s|, \quad (3)$$

where Δ_s is a shift and $|\phi_s\rangle$ is the appropriate partial wave taken at the linearization energy inside the sphere, in this case, the Cu *s* partial wave at its linearization energy.

III. CRYSTAL STRUCTURE

The crystal structure of Cu_{2-x}S is rather complex and the nomenclature somewhat confusing. The various forms all consist of either a cubic or hexagonal close-packed lattice of S atoms with Cu atoms occupying various interstitial sites with different statistical probabilities. One distinguishes different phases depending on the Cu content and depending on the temperature range.

Stoichiometric Cu₂S is called chalcocite, although occasionally, one finds this also spelled as chalcocite.¹⁶ Following Potter,²⁰ one distinguishes three different modifications, a monoclinic phase called low chalcocite below 103.5 ± 1.0 °C, a hexagonal phase called high chalcocite between the previous temperature and 436 ± 10 °C, and a cubic phase above this temperature. The crystal structure of the monoclinic phase was fully determined by Evans²³ and is, in fact, closely related to that of high chalcocite. It is essentially a superstructure of the hexagonal lattice with slight distortions, containing 48 f.u. Cu₂S. For the hexagonal high-chalcocite structure, only a statistical distribution of the atoms over the various Wyckoff sites could be determined, and different authors report somewhat different distributions. For example, Will *et al.*²⁵ include Cu at *2b*, *4f*, *6g*, *6h*, and *2a* sites and S at *2c* sites. As is well known, the Wyckoff sites differ by their local symmetry, and the number indicates how many equivalent sites of this type there are in a unit cell. The crystallographers determine the relative occupancies of these sites by generating the corresponding x-ray diffraction intensities and by searching for a best fit to the data. Wuensch and Burger^{21,22} only include Cu at *2b*, *4f*, and *6g*, while Sadanaga *et al.*²⁶ include atoms at *2b*, *4f* and *12k* positions. As will be discussed later, in the model of Will *et al.*, the distance between the Cu *6h* and S *2c* site is 1.05 Å, which seems unreasonably close. Since all S sites are occupied, it seems that we cannot allow any Cu atoms in *6h* sites. Apparently, such restrictions were not included in the best fit determination.

Cu_{1.8}S is distinguished as a separate phase and is called digenite. Some authors distinguish low digenite and high digenite based on observed phase transitions by differential

thermal analysis, but all crystals identified as digenite are found to be cubic and based on an fcc sublattice of S. This structure is then similar to cubic chalcocite except that only 9/10 of the Cu sites are occupied. The simplest form imaginable for a cubic Cu_2S would be the antifluorite structure, in which the Cu atoms occur in the $8c$ Wyckoff positions, i.e., the $(1/4, 1/4, 1/4)$ positions. However, the Cu atoms apparently do not (or at least not exclusively) occupy this highly symmetric position but instead occupy various other lower symmetry Wyckoff positions, such as the $192l$ sites. Morimoto *et al.* proposed a specific model for Cu_9S_5 based on a rhombohedral cell which corresponds to a $5 \times 5 \times 5$ cubic cell and with atoms at or close to the body diagonal. This unit cell would exactly contain 1 f.u. Cu_9S_5 . This model, however, does not provide the best fit to the diffraction data, and others such as Will *et al.*²⁵ determined different site occupancies over a few different Wyckoff sites, which were furthermore found to differ at different temperatures. All the above models for digenite correspond either to naturally found minerals or to synthetic crystals produced from mixtures of pure Cu and S powders heated in silica vessels and then cooled rapidly. The various phases at different temperatures were obtained by heating the crystal during the diffraction measurement. On the other hand, this does not exclude that crystals of composition $\text{Cu}_{1.8}\text{S}$ could exist in the hexagonal modification. Specifically, the Cu_{2-x}S obtained by the Clevite process,⁵ i.e., by substituting Cu in a CdS wurtzite crystal, is likely to have a hexagonal sublattice of S atoms. Furthermore, this structure appears most relevant to the Cu_2S used in solar cells. For example, all data on the optical absorption and band gaps, to the best of our knowledge, come from hexagonal material. Also, the recently studied nanoparticle Cu_{2-x}S with different x have hexagonal structures.⁹

To keep the nomenclature clear, we will reserve the name digenite for the cubic modification of $\text{Cu}_{1.8}\text{S}$ only and will consider the hexagonal ones simply as Cu-deficient hexagonal high chalcocite. In fact, the cubic form of high chalcocite Cu_2S is also called high digenite according to Will *et al.*²⁵ because above 500 °C, only Cu_2S exists. It thus appears that the terms chalcocite and digenite refer to the hexagonal and cubic forms, respectively, regardless of the exact composition. To be unambiguous, we will use the terms cubic and hexagonal chalcocite when we refer to Cu_2S and digenite for the cubic form of $\text{Cu}_{1.8}\text{S}$. Another form of Cu-deficient hexagonal chalcocite is known with a separate name, namely, $\text{Cu}_{1.96}\text{S}$, which is known as djurleite.²⁷ A full structure determination of djurleite was carried out by Evans.²³ Similar to low chalcocite, it is a monoclinic structure and can again be considered as a superstructure of hexagonal chalcocite with just a slightly reduced Cu concentration. The djurleite unit cell corresponds to $\text{Cu}_{62}\text{S}_{32}$, i.e., just two Cu atoms missing from a 32 f.u. Cu_2S .

To complete the discussion of Cu_{2-x}S , we mention that CuS is known as covellite. Its structure and electronic structure were studied by Gotsis *et al.*²⁸ It is also a hexagonal structure consisting of alternating layers of CuS and $\text{Cu-S}_2\text{-Cu}$.

In summary, for our present purposes, it appears necessary to consider both hexagonal and cubic underlying S lat-

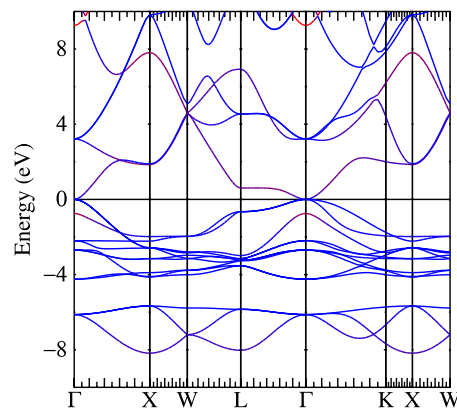


FIG. 1. (Color online) Energy bands of Cu_2S in the antifluorite structure and the LDA with the Cu s band highlighted in red. The k points shown correspond to the usual fcc Brillouin zone.

tices. It seems reasonable to start with the simplest cubic antifluorite structure. Although this was never observed to be the true crystal structure, it serves as a high-symmetry starting point from which to discuss the cubic modifications of high chalcocite and digenite. Finally, we need to consider at least a few different Cu compositions because experimentally, a clear correlation between Cu content and band gap has been found. Except for monoclinic low chalcocite and djurleite, no full structural models are available, so we will need to construct models first to reproduce as possible the observed Wyckoff site occupancies. This is described below in Sec. IV B.

IV. RESULTS

A. Antifluorite band structure

The first and the simplest model we consider for Cu_2S is the perfect antifluorite (AF) structure. Full-potential LDA calculations give the optimal lattice constant of 5.45 Å, about a 3%–5% underestimate with respect to the experimental lattice constant of digenite (5.57 Å) (Ref. 25) or cubic chalcocite (5.762 at 500 °C) (Ref. 25) with the corresponding cohesive energy of -12.69 eV. We plot the LDA band structure for this case in Fig. 1 calculated at the theoretical equilibrium lattice constant. For the moment, ignore the color coding of the bands, which will be explained shortly.

It is clear that this system is metallic or semimetallic. At first sight, it seems to have a zero band gap, but we will argue shortly that one should rather consider it to have a negative band gap of -1 eV (or overlap of 1 eV) at the Γ point. This contradicts with the experimental results of the semiconducting nature of the Cu_2S .^{7,16–18} One possible reason for this contradiction is that the AF structure is strongly oversimplified compared to the experimentally reported structures. However, LDA is known to underestimate band gaps and may turn a small band gap semiconductor into a semimetal. Typically, for example, the binding energy of Cu d bands might be expected to be underestimated by LDA and this may lead to an underestimate of the gap if there are

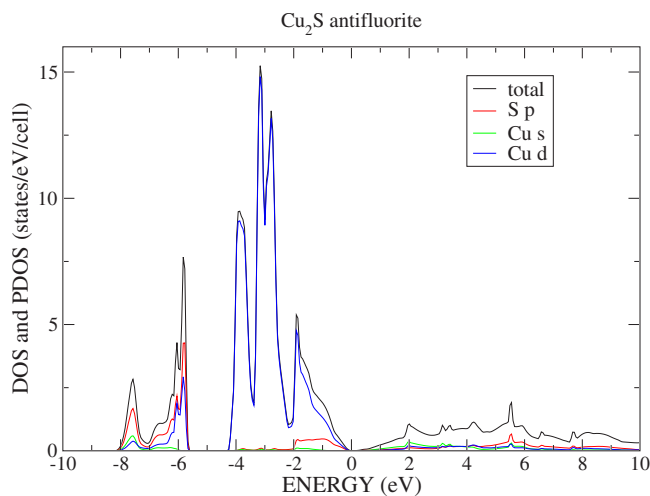


FIG. 2. (Color online) Partial densities of states for Cu_2S in the antifluorite structure obtained in the LDA.

anion p states above it that are interacting with it.

A first important step is to identify the nature of the bands by inspecting the partial densities of states (PDOS). Figure 2 shows that the nature of the valence band maximum (VBM) is predominantly Cu d -like. A similar nature of the VBM is also observed for other Cu compounds, such as Cu_2O and CuBr . Comparison of our calculated PDOS with experimental photoemission data for Cu_2O (Ref. 41) and CuBr (Ref. 42) shows that our densities of states are in good agreement with the x-ray photoelectron spectroscopy spectra, without significant downward shifts of Cu d with respect to the Fermi level. Thus the same can be expected for Cu_2S .

More details on the nature of the bands are obtained by plotting the bands with a color in proportion to the weight of certain atomic orbitals. In Fig. 1, the bands are colored red in proportion to the Cu s contribution to the eigenvector at each k point with blue as the complementary color. Thus, completely blue means zero Cu s , while entirely red means 100% Cu s . Similarly, in Fig. 3, the Cu d contribution to the bands is highlighted.

These plots clearly reveal that the lowest conduction band has a strong Cu s component except right near the center of

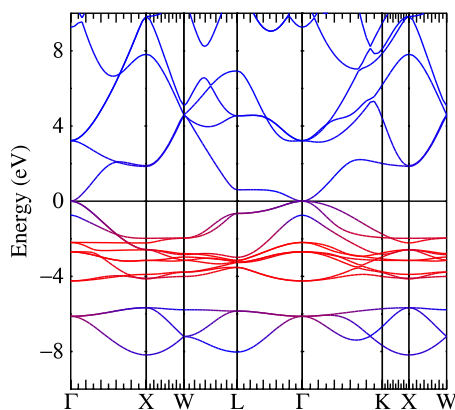


FIG. 3. (Color online) Cu_2S , AF, the Cu d contribution to the bands is highlighted in red.

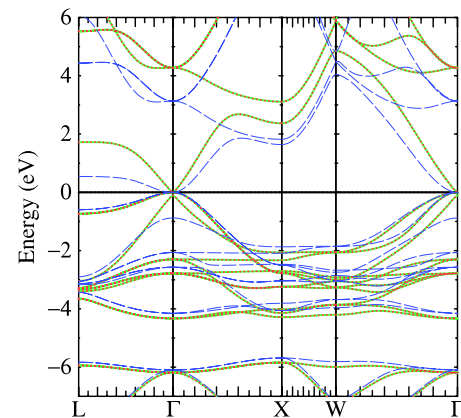


FIG. 4. (Color online) Comparison of QSGW (green solid) with LDA (blue dashed) bands for Cu_2S in the AF structure.

the Brillouin zone where the Cu s band occurs below the triply degenerate VBM. The latter is clearly a predominantly Cu d -like state. This suggests that the Cu s band has in some sense crossed the Cu d band, and the apparent zero band gap is due to the degeneracy of the Cu d band at Γ . If Cu s -like states were to move up somewhat above the Cu d -bands in a more accurate treatment than LDA, possibly a gap could open.

To check this possibility we next performed calculations of AF Cu_2S using the QSGW approach. In Fig. 4, the QSGW and LDA results are compared with each other. The Cu s state at the Γ point is indeed seen to move up by about 0.8 eV but not enough to open a gap. Thus, QSGW calculations confirm the metallic nature of hypothetical AF Cu_2S . The “quasiparticle self-consistency” aspects of QSGW are important here. In LDA, the band gap, defined as $\Gamma_{1c} - \Gamma_{15v}$, is -0.88 eV; in $G^{\text{LDA}}W^{\text{LDA}}$, it is -0.41 eV; in $G^{\text{LDA}}W^{\text{LDA}}$ but setting the quasiparticle renormalization factor³³ $Z=1$, which is often found to be a better approximation, we obtain -0.29 eV; and, finally, with QSGW, we find -0.11 eV. Based on experience with other semiconductors and, in particular, with CuBr ,³³ we expect this to be accurate to within 0.1 eV.

The above comparison suggests that at least in part, we can overcome the LDA error by shifting up the Cu s states. In Fig. 5, we compare the bands of antifluorite Cu_2S in QSGW with the LDA+shift results in which only the Cu s partial waves are shifted up. This shows that we can now indeed reproduce the correct position of the Cu s vs Cu d VBM at the Γ point, but we still underestimate the conduction band at k points away from Γ and overestimate the bands deeper in the valence band. Thus, it provides a way to somewhat correct LDA but does not entirely reproduce GW.

The fact that the VBM is triply degenerate suggests that to explain the semiconducting nature of Cu_2S , the distortions from the high-symmetry AF structure are essential. One might expect that these will break the degeneracy of the Cu d state at Γ and hence possibly open a small gap. To test this idea, we first considered a simple cubic Cu_8S_4 cell based on the antifluorite structure but with small random displacements of the Cu atoms away from the $(1/4, 1/4, 1/4)$ position. The displacements taken were of order of 0.05–0.10 in

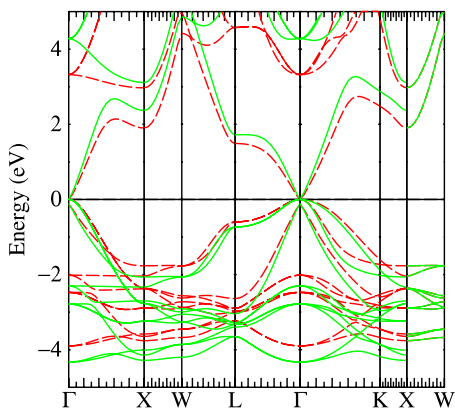


FIG. 5. (Color online) Band structure of antifluorite Cu_2S . Comparison of QSGW (green solid) with LDA+Cu s shift (red dashed).

reduced coordinates. It was found that indeed this opened a small band gap of order of 0.2 eV, as can be seen in Fig. 6. Furthermore, it now becomes clear that the lowest conduction band is Cu s -like even at the Γ point. Thus, shifting Cu s states upward by about 0.8 eV as suggested by the QSGW calculation for AF could lead to a gap of order 1 eV. Since this structure is still rather unrealistic, we do not describe it in further detail.

B. Weighted random number generated structures

In order to obtain a more realistic description of the electronic structure, we first need to create structural models that take the structural complexity into account and agree as close as possible with the x-ray diffraction studies. To this end, we developed a “weighted random number” algorithm. In order to be able to still use a standard band-structure approach, we continue to use periodic boundary conditions but construct a supercell. This supercell then contains a large enough number of sites of each Wyckoff site type that we can occupy some of them with Cu atoms and leave others empty in the same proportion as dictated by the experimental observations. At the same time, we need to make sure that the atoms are staying within a reasonable distance from each other. For example, in the cubic chalcocite structure (at 500 °C), Will *et al.*²⁵ find that Cu atoms occur in three types of Wyckoff positions, $8c$ with representative coordinates $(1/4, 1/4, 1/4)$ and occupancy $2.06/8$, $4b$ with representative coordinates $(1/2, 1/2, 1/2)$ and occupancy $0.38/8$, and $192l$ with representative coordinates $(0.1067, 0.166, 0.2826)$ and occupancy

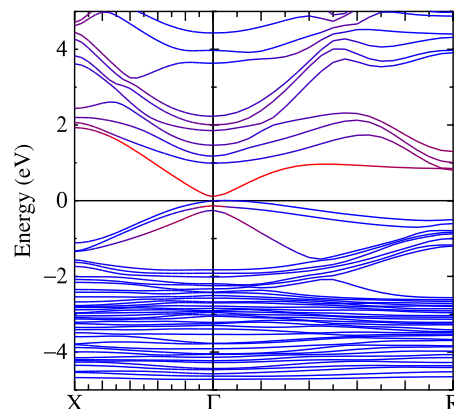


FIG. 6. (Color online) Energy bands of Cu_2S in a structure slightly distorted from antifluorite. The k points are $X = \frac{\pi}{a}(1, 0, 0)$ and $R = \frac{\pi}{a}(1, 1, 1)$.

$5.56/8$. The S atoms occur at the $4a$ positions $(0,0,0)$ with $4/4$ occupancy. These numbers refer to the conventional cubic fcc unit cell, i.e., a cube with S atoms on the corners and in the face centers. If we construct a $2 \times 2 \times 2$ supercell, it will contain 32 S and 64 Cu atoms. This means that we have, for example, $8 \times 192 = 1536$ l -type positions in our supercell. Out of these, only $(5.56/8)64 \approx 44$ should be occupied by a Cu atom. To generate such a structure, we start by listing the different types of Wyckoff positions, in this case, c , b , and l , and assigning an interval of length equal to its relative occupancy to each, such that their total adds up to an interval of length 1 when stacked together. We then pick a random number with uniform distribution between 0 and 1, and depending on which interval it falls in, we decide to place an atom in the corresponding Wyckoff type. For instance, if the random number lies between 0 and $2.06/8$, we assign it to the c type; if it lies between $2.06/8$ and $(2.06+0.38)/8$, we assign it to b ; and if it is higher than $2.44/8$, we assign it to an l position. Next, a second random number generator picks any of the equivalent Wyckoff sites available of that type in the entire cell. For example, if we had an l position, we pick an integer random number between 1 and 1536 and accordingly pick the specific site to place the first Cu atom. Then, we repeat this procedure but in each step, we check that the chosen site is not closer to any of the previously placed Cu atoms or the S positions than a reasonable cutoff distance. If this criterion is not satisfied, we reject the specific position and pick a new random number but of the same type. Of course, we check the distance not only to atoms in the cell

TABLE I. $\text{Cu}_{64}\text{S}_{32}$ cubic supercell: experimental (Ref. 25) and computer generated occupancies and reduced coordinates of one of the representative Wyckoff positions in the cell (space group $225 Fm\bar{3}m$).

Atom	Wyckoff site	Expt. (%)	Model (%)	Number of atoms	x	y	z
S	$4a$	100	100	32	0	0	0
Cu(1)	$8c$	25.75	25.0	16	0.25	0.25	0.25
Cu(2)	$4b$	4.75	3.1	2	0.5	0.5	0.5
Cu(3)	$192l$	69.5	71.9	46	0.1067	0.166	0.2826

TABLE II. $\text{Cu}_{58}\text{S}_{32}$ digenite-400 supercell: experimental (Ref. 23) and computer generated occupancy. The positions are the same as in Table I.

Atom	Wyckoff site	Expt. (%)	Model (%)	Number of atoms
S	4a	100	100	32
Cu(1)	4b	2.8	1.7	1
Cu(2)	8c	27.8	29.3	17
Cu(3)	192l	69.4	69.0	40

but also to their image positions in the neighboring cells obtained from the periodic boundary conditions. We repeat this procedure for a certain number of iterations until all atoms are placed. The cutoff distances are adjusted if necessary. Finally, the resulting structure is visually inspected using the XCRYSDEN program.⁴³

Using this procedure, we generated structures for cubic chalcocite, hexagonal chalcocite, and digenite. The resulting cells and their occupancies of Wyckoff sites are compared with the experimental ones in Tables I–III.

For digenite, Will *et al.*²⁵ give a slightly different occupancy for the structure at 300 °C than at 400 °C. The difference is that at 300 °C, no atoms were found in the 4b position. We constructed a model for both; the only difference is that at 300 °C, we have 18 atoms at 8c positions and none at 4b.

We note that for hexagonal chalcocite, we used experimental data from Wuensch and Buerger²¹ because in the structure proposed by Will *et al.*,²⁵ Cu atoms are placed in 6h positions which occur too close to S atoms to be realistic. Also, Wuensch and Buerger proposed that the S atoms sit in the 2d instead of 2c positions, but these again are too close to some of the Cu atoms. We thus chose the crystallographically equivalent 2c positions. The cubic and hexagonal chalcocite structures are shown in Figs. 7 and 8, respectively. Full structural data can be obtained from the authors upon request. One may notice that the hexagonal structure has a layered look with alternating layers of mixed Cu-S and pure Cu layers. The same type of structure is observed in the monoclinic low-chalcocite form²³ shown in Fig. 9 and in the djurleite structure^{23,27} and even in covellite.²⁸ Such layers can also be recognized to exist in the cubic form along the (111) close-packed planes in Fig. 7.

C. Band structure of model structures

In Fig. 10, we show the band structure of the hexagonal chalcocite $\text{Cu}_{32}\text{S}_{16}$ model both in the LDA and including a

shift of the Cu *s* partial waves taken equal to that used for the antifluorite structure. The Cu *s* character of the bands is highlighted in red. The lattice constant was taken to be the experimental one as given in Will *et al.*,²⁵ $a=4.033$ Å, $c/a=1.6709$. We can see that in LDA, only a very small band gap of about 0.04 eV opens at the Γ point between Cu *s*-like conduction band and a Cu *d*-like valence band, similar to the situation we had for the slightly distorted antifluorite structure. Adding the Cu *s* shift leads to a larger gap of 0.50 eV at the Γ point. We may also notice that the conduction band at Γ is still Cu *s*-like, but along the Γ -*M* axis, another band which has no Cu *s* character crosses this band and has a minimum at about the same value of 0.5 eV. So, the system is close to a direct to indirect crossover. Still, this value is significantly smaller than the experimental gap reported for chalcocite, which is about 1.2 eV. We will address the possible origins of this discrepancy in Sec. V.

By fitting a parabola to the bands near the Γ point, we can make a rough approximation to the effective masses. For our $\text{Cu}_{32}\text{S}_{16}$ model, we obtain the effective electron mass $m_e^* \approx 0.3$ and the hole mass $m_h^* \approx 0.8$. We ignore here the anisotropy of the mass tensor and only consider the curvature along the Γ -*M* direction. This leads to an approximate exciton mass m_x , given by

$$\frac{1}{m_x} = \frac{1}{m_e^*} + \frac{1}{m_h^*}, \quad (4)$$

of 0.2. These values are important to give guidance to some of the intended applications of Cu_2S nanoparticles and for solar cell applications. These values are rather typical for semiconductors.

For the monoclinic structure, we find an LDA gap of 0.024 eV, while adding the Cu *s* shift gives us a band gap of 0.58 eV. The experimental lattice constants were used for this calculation.

Similar results are obtained for the cubic cell as can be seen in Fig. 11. This calculation was done at the experimental lattice constant of $a=5.762$ Å, corresponding to cubic chalcocite at 500 °C. After the Cu positions were determined by the weighted random number generator algorithm, they were relaxed using a conjugate gradient method. This allows atoms to settle into their equilibrium positions but only slightly changes them, so that the occupancy of the Wyckoff sites does not change. Little change in the band structure is obtained between the initial and relaxed structures. Including the Cu *s* shift, we obtain a direct gap at Γ of 0.40 eV. The valence band maximum is found to move away from Γ to

TABLE III. $\text{Cu}_{32}\text{S}_{16}$ hexagonal supercell: experimental (Ref. 21) and computer generated occupancies and positions (space group 194 $P6_3/mmc$).

Atom	Wyckoff site	Expt. (%)	Model (%)	Number of atoms	<i>x</i>	<i>y</i>	<i>z</i>
S	2c	100	100	16	2/3	1/3	1/4
Cu(1)	2b	43.5	43.7	14	0	0	1/4
Cu(2)	4f	35.5	31.3	10	1/3	2/3	0.568
Cu(3)	6g	21.0	25.0	8	0	1/2	0

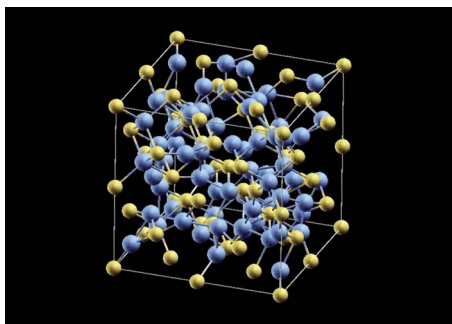


FIG. 7. (Color online) Cubic chalcocite $\text{Cu}_{64}\text{S}_{32}$ model cell. Large blue spheres, Cu; small yellow, spheres, S.

ward the $R=(\pi/2a)(1, 1, 1)$ point, and a slightly smaller indirect gap of 0.35 eV is found. The conduction band mass in this case was found to be somewhat larger, $m_e^* \approx 0.37$, and the valence bands are too flat to obtain a reasonable estimate from the k -point values we have calculated, indicating a very high hole mass in this case.

Next, we present results for models with $x \neq 0$ (Fig. 12 and 13). First, we consider the cubic digenite structure. This structure can be considered as containing 10% vacancies. We studied both the 300 and 400 °C models of Will *et al.*, but both gave very similar band structures as expected since they differ only in whether the $4b$ site has a slight occupation or not. We show the results only for the 300 °C (in Fig. 12).

It is notable that a much higher band gap (about 0.8 eV) is obtained than for chalcocite even in the LDA. Adding the Cu s shift, however, does not add much: it becomes 1.06 eV. Furthermore, we can see that now the Fermi level lies about 0.3 eV below the VBM. Since optical transitions can only take place between filled and empty states, and assuming that only vertical transitions occur, this means that the onset of optical absorption occurs at 1.37 eV. We conclude that adding Cu vacancies increases the band gap directly as well as through the Moss-Burstein effect.^{44,45} The direct increase in the gap can be traced back to arise mainly from a reduction in the valence bandwidth. If one aligns the bottom of the

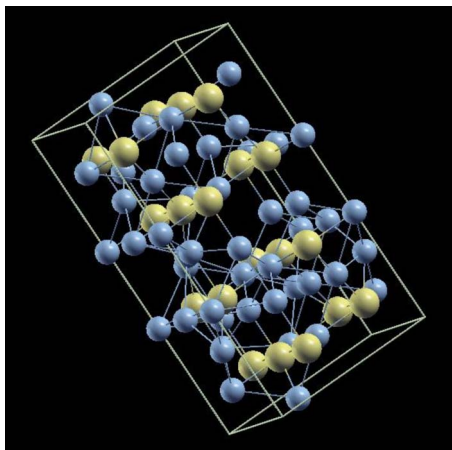


FIG. 8. (Color online) Hexagonal chalcocite $\text{Cu}_{32}\text{S}_{16}$ model cell. Small blue spheres, Cu; large yellow spheres, S.

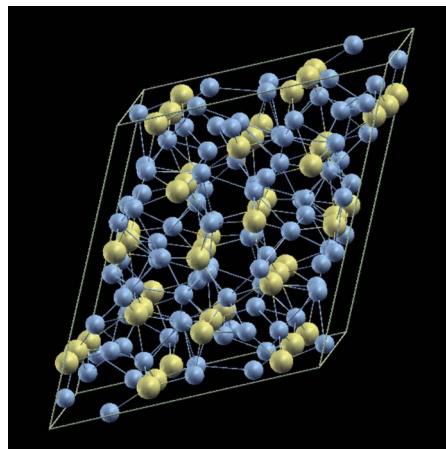


FIG. 9. (Color online) Monoclinic chalcocite $\text{Cu}_{96}\text{S}_{48}$ cell. Small blue spheres, Cu; large yellow spheres, S.

valence bands and simultaneously the S s -like deeper valence bands, one can see in a density of states (DOS) plot that the conduction band minima align but the VBM is reduced in energy. Clearly, by reducing the number of Cu at-

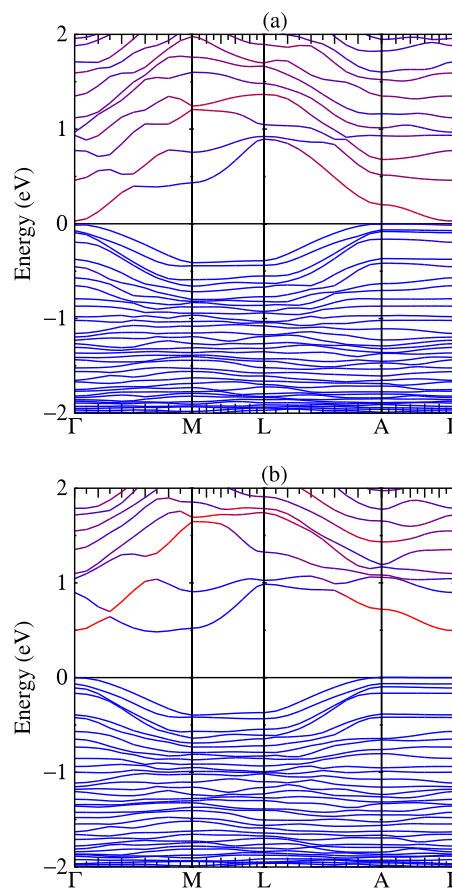


FIG. 10. (Color online) Energy band structure of hexagonal chalcocite model $\text{Cu}_{32}\text{S}_{16}$ in LDA (top) and with Cu s shift (bottom). The Brillouin zone has the usual hexagonal high-symmetry points but with twice the lattice constant so all reciprocal k lengths are halved.

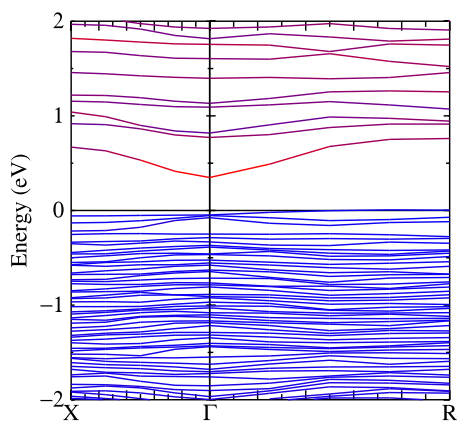


FIG. 11. (Color online) Energy bands of cubic chalcocite model $\text{Cu}_{64}\text{S}_{32}$ including Cu s shift and highlighting Cu s in red. The k points are $X = \frac{\pi}{2a}(1, 0, 0)$ and $R = \frac{\pi}{2a}(1, 1, 1)$.

oms, Cu d bands are removed from near the VBM, which consists of antibonding combinations of Cu d bands with S sp . This is similar to an effect noticed by Persson and Zunger for CuInSe_2 .⁴⁶ They showed a lowering of the valence band maximum near surfaces and interfaces where the Cu coordination is reduced.

Next, we consider our hexagonal models in which we remove either 1, 2, or 3 randomly selected Cu atoms. These models correspond to 3.125%, 6.25%, and 9.375% Cu vacancies. As an example, the band structure of the $\text{Cu}_{30}\text{S}_{16}$ is shown in Fig. 13. As in cubic digenite, the gap increases and, secondly, the Fermi level moves below the valence band maximum. The system strictly speaking becomes metallic. One can consider it as a heavily p -type doped material. This leads to a further increase of the effective optical gap through the Moss-Burstein effect.^{44,45}

In Table IV, we summarize our results on the band gaps obtained thus far. Because essentially, the band gap in all materials appears to be direct or close to the smallest direct gap, we define the gap as $E_g = E(\Gamma_{CBM}) - E(\Gamma_{VBM})$. We define the conduction band minimum (CBM) as the first empty band with positive mass and the valence band maximum as

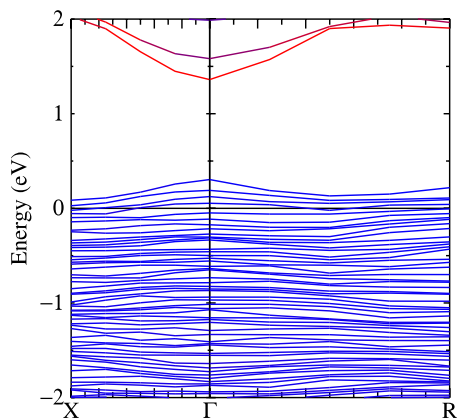


FIG. 12. (Color online) Energy band structure of $\text{Cu}_{58}\text{S}_{32}$ digenite-300 including Cu s shift. The k points are the same as in Fig. 11.

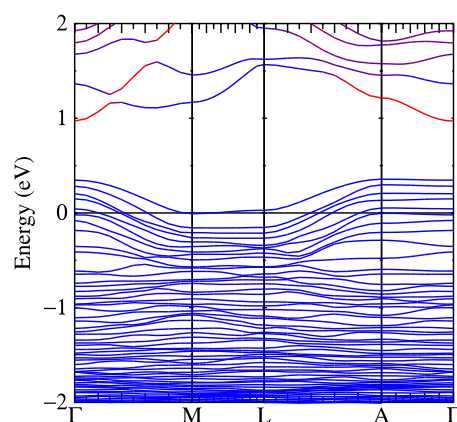


FIG. 13. (Color online) Energy band structure of hexagonal $\text{Cu}_{30}\text{S}_{16}$ including Cu s shift and highlighting Cu s band contribution in red.

the highest band with negative mass below it. Usually, there is a level at Γ or close to Γ just below the Fermi level. The Fermi level in each of these cases was calculated from a $2 \times 2 \times 2$ k -point mesh using the tetrahedron method even though the self-consistent calculations were done with a single shifted k point. In Table IV, the position of the Fermi level E_F is given relative to the VBM. The onset of optical absorption is labeled as E_a and is the difference between the CBM and the Fermi level.

First, considering the three structures, we can see that the gap increases from cubic to hexagonal to monoclinic. Second, considering the effect of Cu concentration, we can see that the gap increases with decreasing Cu content. The gap increase is even more spectacular in the cubic case. We should also keep in mind that digenite corresponds to the highest concentration of Cu vacancies considered, namely, 10%. Nevertheless, the Fermi level does not move so deep below the VBM because the density of states is higher near the VBM in cubic compared to in hexagonal materials as we have already seen from the effective masses. The increase in gap with decrease in Cu content qualitatively agrees with experimental reports.^{7,16} For $\text{Cu}_{1.8}\text{S}$, a gap as high as 1.75 eV was reported.¹⁵

To assess the effects of the uncertainty in the structure on the gaps, we have repeated the calculations for digenite with a slightly different structure, which, however, generated the

TABLE IV. Band gaps and related quantities in various Cu_{2-x}S models, including Cu s shift correction.

Structure	E_g	E_F	E_a
Hexagonal $\text{Cu}_{32}\text{S}_{16}$	0.50	0.00	0.50
Hexagonal $\text{Cu}_{31}\text{S}_{16}$	0.55	-0.34	0.88
Hexagonal $\text{Cu}_{30}\text{S}_{16}$	0.62	-0.35	0.97
Hexagonal $\text{Cu}_{29}\text{S}_{16}$	0.66	-0.42	1.08
Monoclinic $\text{Cu}_{96}\text{S}_{48}$	0.58	0.00	0.58
Cubic chalcocite $\text{Cu}_{64}\text{S}_{32}$	0.40	0.00	0.40
Cubic digenite $\text{Cu}_{58}\text{S}_{32}$	1.06	-0.32	1.38

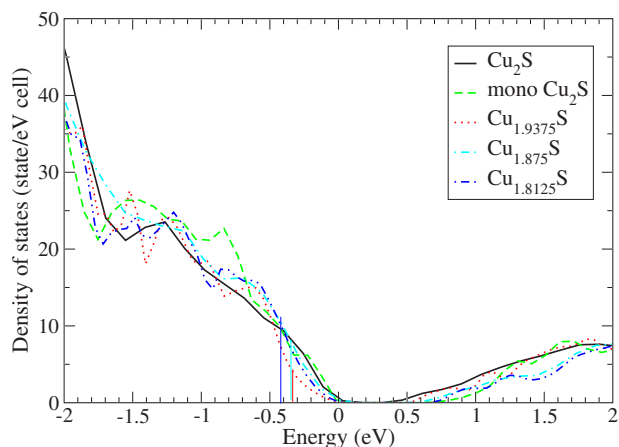


FIG. 14. (Color online) Total density of states in various structures of Cu_{2-x}S . The Fermi level is indicated by the vertical lines for the $x \neq 0$ cases.

same statistical distribution, i.e., the same number of atoms on each type of Wyckoff site. The band gaps differed by less than 0.1 eV. The Fermi level positions in the valence band also differed by less than 0.1 eV. This structure gave a 0.1 eV higher LDA gap but a 0.07 eV lower Fermi level position below the VBM, so the net difference in optical gap was only 0.03 eV. Adding gap corrections does not alter this finding. Thus, we conservatively conclude that the error bar arising from statistical fluctuations in the structure is at most 0.1 eV.

In Fig. 14, we plot the total density of states of various models. The valence band maxima are aligned and the position of the Fermi level is indicated for the cases with $x \neq 0$. From the area under the curve between the VBM and the Fermi level, we can make a rough estimate of the hole concentration. For example, for $\text{Cu}_{31}\text{S}_{16}$, we obtain 0.6 holes per unit cell, which amounts to $8 \times 10^{20} \text{ cm}^{-3}$. This also makes sense because we essentially removed ten d states with the Cu atom but 11 electrons, so we have about one hole left in the VBM. For the other cases, we obtain indeed approximately two and three times this value. These hole concentrations are comparable to the ones obtained in the study by Partain *et al.*⁷ of Cu_2S exposed to heat treatments in moist air lasting from 1 h to a few hours.

Considering next a DOS in the conduction band region, we may notice that the DOS is fairly low near the minimum, but at about 0.5 eV above the CBM, an increase with a peak occurs and another one occurs 0.5 eV higher. This corresponds to the onset of contributions to the DOS from the higher conduction bands as can be seen by comparison with the band plots.

Finally, in Fig. 15, we plot Cu PDOS for the hexagonal $\text{Cu}_{32}\text{S}_{16}$ model. We can see that the dominant contribution in the valence band is Cu d . In the conduction band, Cu s and Cu p states seem to have about equal weights, but they are about ten times lower than the d -DOS near the VBM. Because of the dipole selection rule $\Delta l = \pm 1$, we can expect mainly Cu d to Cu p -like transitions near the gap.

D. Total energy differences

The cohesive energies per Cu_2S unit for the various structures are summarized in Table V. The lowest energy is found

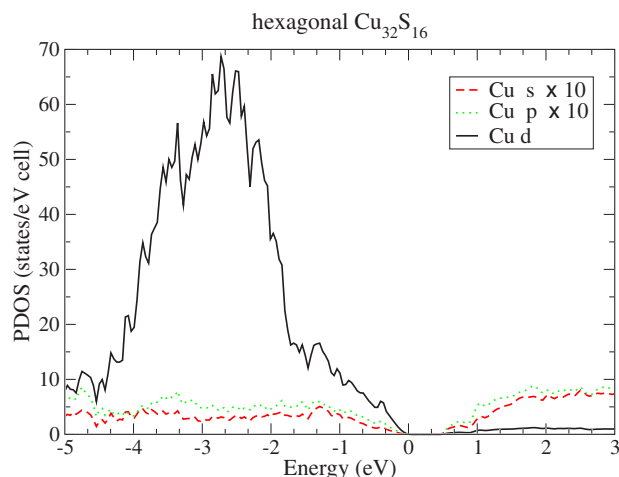


FIG. 15. (Color online) Partial densities of states in hexagonal $\text{Cu}_{32}\text{S}_{16}$.

for the monoclinic structure. This is in agreement with the fact that this is the structure observed at low temperature. We can tentatively correlate the ordering in terms of increasing energy with the temperature ranges in which the different structures occur. Experimentally,²⁵ one finds the hexagonal form to be the stable form in the range 103–436 °C and the cubic form at high temperature. To compare stability of different structures at different temperatures, we should compare free energies $E - TS$ instead of the energies at zero temperature calculated here. The question becomes at what temperature the entropy term overcomes the energy differences. The entropy arises presumably primarily from phonons and, in particular, in this system from the high mobility of the Cu atoms. Assuming that the vibrational entropy is higher for the hexagonal than for the monoclinic case and still higher for the cubic case, one could tentatively draw the schematic diagram given in Fig. 16. Calculating the vibrational contributions to the free energy as function of temperature is beyond the scope of this study. The diagram is only a suggestion.

The antifluorite structure has the highest energy, and this is consistent with the fact that the ordered cubic structure is not preferred. As was mentioned before, the cubic chalcocite can be viewed as Cu atoms in slightly irregular positions in the S lattice rather than all rigidly placed at the high-symmetry $8c$ Wyckoff positions.

Comparing the total energies of the structures with Cu vacancies requires a consideration of the chemical potential μ_{Cu} for Cu atoms. If we take the latter to be their cohesive

TABLE V. Cohesive energies in Cu_2S for different structures.

	E_{coh} (eV/ Cu_2S)
Monoclinic	-12.99
Hexagonal	-11.44
Cubic	-11.06
Antifluorite	-10.50

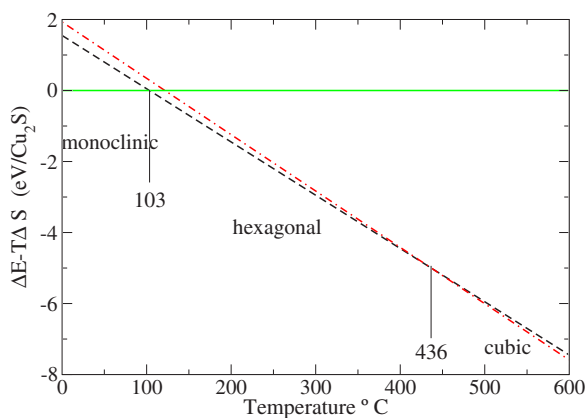


FIG. 16. (Color online) Schematic diagram of free energy versus temperature for different phases of Cu_2S .

energy in bulk fcc Cu, i.e., assuming thermodynamic equilibrium with a bulk Cu reservoir, we can calculate

$$\Delta E(n) = E(\text{Cu}_{32-n}\text{S}_{16}) - E(\text{Cu}_{32}\text{S}_{16}) + n\mu_{\text{Cu}} \quad (5)$$

as a measure of the stabilization of the system by Cu vacancies. Using $\mu_{\text{Cu}} \approx 4.3$ eV/atom, we obtain $\Delta E(n)$ to be -3.0 , -3.6 , and -2.6 eV for $n=1, 2, 3$. Normalizing per Cu_2S unit, this comes down to -0.19 , -0.22 , and -0.16 eV. The fact that these numbers are negative means that the system favors introducing some vacancies when in equilibrium with bulk Cu. In other words, the Cu atoms will rather go to the bulk Cu than staying in the Cu_2S . This indicates an intrinsic instability of Cu_2S , which is an important qualitative result. For example, in an oxidizing environment, one might want to use the chemical potential of Cu in a copper oxide, such as Cu_2O . This will be even more negative than in bulk Cu and thus it will be even more favorable to move a certain number of Cu atoms from Cu_2S to Cu_2O . This is consistent with the known problem of long-term instability of Cu_2S in air, in particular, in oxidizing environments.

V. DISCUSSION

One of the main goals of our paper is to determine the band gap of the system and the nature of the band gap, direct or indirect. Experimentally, the information on band gaps is mainly concerned with hexagonal materials obtained by the Clevite process. The most reliable measurement is probably the photoconductivity measurement of McLeod *et al.*¹⁹ which gave 1.18 ± 0.03 eV. Most of the information on the nature of the band gap comes from optical absorption measurements. However, all of these studies show a considerable amount of free-carrier absorption, more specifically due to holes associated with a certain degree of nonstoichiometry, i.e., the presence of Cu vacancies. Thus, the optical absorption does not really go to zero but only through a minimum between the interband and intraband absorption. This makes extracting a reliable band gap value difficult. Typically, what most authors^{7,16} do is to model the Drude-like low energy absorption and subtract it from the data. After this subtraction, the remaining absorption coefficient α is then plotted

either as $\sqrt{\alpha}$ or as α^2 as function of photon energy. A linear behavior in the former case is considered as evidence for an indirect band gap and a linear behavior in the latter case is taken as evidence for a higher energy direct gap. In this way, for example, Partain *et al.*⁷ arrive at a lowest indirect gap of 1.16 eV, followed by a direct gap of 1.28 eV. Furthermore, they find another change in slope in the α^2 versus energy curve at 1.8 eV, which indicates the presence of a second direct absorption onset, which they ascribe to a second deeper lying valence band with maximum at Γ . Other authors have arrived at slight variants of this scheme as discussed by Partain *et al.*⁷

Before comparing with our results, we should note that the question of a direct or indirect gap is somewhat questionable in this material if one takes the strongly disordered nature of this material into account. The fact that Cu atoms are somewhat randomly distributed among different Wyckoff sites means that, strictly speaking, there is no periodicity, and hence, one can expect violation of momentum conservation in optical transitions to some extent. Secondly, the unit cells we need to obtain a reliable model of the structure are rather large. This means that k points which would be at the Brillouin-zone edge of the simple cubic or hexagonal structure are now folded on the Γ point and become direct.

Closer inspection of the experimental data reveals that near the minimum, the optical absorption coefficient is typically still of order of 10^4 cm^{-1} . This is high for an indirect transition. In Si, for example, the optical absorption coefficient, a few 0.1 eV above the onset, is 2 orders of magnitude smaller.⁴⁷ The only reliable way of determining the indirect nature of a band gap is to study its low temperature behavior and identifying the separate onsets for phonon absorption and emission. The subtraction of the Drude-like absorption adds considerable uncertainty and makes it effectively impossible to determine the nature of the gap. Sure enough, plotting $\sqrt{\alpha}$ as function of photon energy emphasizes the low energy region absorption, whereas plotting α^2 as function of photon energy suppresses this region. Thus, it is no surprise that one finds somewhat higher onsets for the latter plot. Given the uncertainties of the subtraction of the free-carrier absorption, however, one cannot really consider this as reliable evidence for the presence of a direct and an indirect gap.

In our calculations, we find a direct gap at Γ for all the hexagonal and hexagonal based materials, including the monoclinic case. Only for the cubic chalcocite did we find a slightly higher VBM away from the Γ point, but this is most likely unrelated to the experimental observations of Partain *et al.*⁷ and Mulder¹⁶ which were all concerned with hexagonal material.

Considering the DOS in Fig. 14, we already noticed the increase in DOS at about 0.5 eV above the CBM. This could well explain the observation of a second direct onset as found in the experimental results.⁷ It turns out, however, that this is due to transitions to higher conduction bands rather than from a deeper valence band as suggested by the experimentalists.⁷

For pure Cu_2S , we found a minimum direct gap of 0.5–0.6 eV if we include the monoclinic structure. As mentioned earlier, the monoclinic structure is essentially a superstructure closely related to the hexagonal structure. We

should keep in mind that our model for hexagonal Cu_2S is still only a representative model with about the right distribution of atoms over the Wyckoff sites, but there is still possibly quite some uncertainty on the actual band gap due to slight variations in the positions of the atoms. We estimate this to be of order of 0.1 eV. Under these circumstances, one can actually expect an exponentially decaying band gap tail. This situation is commonly observed in material with a large number of point defects or in amorphous material and is sometimes called an Urbach tail. It leads to a relatively weak absorption coefficient with a cutoff that is difficult to determine precisely. In fact, the DOS near the CBM is relatively weak. Thus, one possibility is that the gap of pure Cu_2S is indeed somewhat lower than previously thought experimentally. The low absorption tail could possibly be hidden under the subtracted Drude absorption. In that case, the reported optical gaps might correspond to our higher onsets, i.e., the peaks in conduction band DOS at ~ 0.5 and ~ 1.0 eV higher than our minimum gap. These could then correspond to the experimental minimum gap and their second onset. Ultimately, however, we do not believe it to be the case based on the following observations on nanoparticles.

Recent studies on nanoparticles of $\text{Cu}_{1.8}\text{S}$ have shown a broadband luminescence peaking at energies of about 2.39–2.52 eV depending on the size of the particles.^{9,11} In nanoparticles, one expects an upward shift of the gap due to size quantization,

$$\Delta E_g = \frac{\hbar^2 \pi^2}{2m_x R^2}, \quad (6)$$

with R the radius of the particle and m_x the exciton mass. For $\text{Cu}_{1.8}\text{S}$, a gap of 1.75 eV was reported.¹⁵ With our estimated masses from the previous section, we can estimate that a 0.55 eV shift is possible for a 1 nm diameter particle and would lead to 2.3 eV. We do not exactly know the size of the particles, but they are unlikely to be much smaller. Unlike absorption, luminescence can easily arise from below band gap states but can hardly overestimate the gap. Thus, it appears that our gaps are really still underestimated by about 0.6 eV. For Cu_2S , we obtain as highest possible estimate the value of the monoclinic phase, which is 0.6 eV, while the experiment indicates 1.2 eV. For $\text{Cu}_{1.8}\text{S}$, we obtain a value of 1.1 ± 0.1 eV, which then seems consistent with an optical gap of 1.7–1.8 eV experimentally.

It is, in fact, likely that our calculation still suffers from the LDA problem of underestimating the band gap. As we saw in Sec. IV A, the shift of Cu s -like states did not fully agree with the QSGW band structure and, in particular, still underestimates the conduction band at points away from Γ . We also found in Fig. 15 that the states near the conduction band minimum also have considerable Cu p -like character. Furthermore, with our procedure, we have only shifted up the Cu s partial waves inside the spheres in energy, but a considerable part of the conduction band wave function may correspond to the interstitial region. All of this makes it likely that we are still underestimating the gap correction. It might be possible to add a more complete self-energy correction by additional shifts, but we have not yet attempted this.

While our calculations apparently are not yet accurate enough to reproduce the absolute gaps, they may be expected to be more reliable to estimate gap changes between different structures. An important insight is that the presence of Cu vacancies not only leads to p -type doping and hence the Moss-Burstein effect but also to a direct opening of the gap. Our models with 3%–9% vacancies led to optical gaps of order of 1.0–1.3 eV. About 0.2–0.4 eV of that gap increase is due to the placement of the Fermi level below the VBM, i.e., the Moss-Burstein effect, but this still leaves about 0.1–0.2 direct effect on the gap. It is fair to say that most real samples have some residual Cu vacancies and are not exactly Cu_2S . In fact, for example, the starting system in the study of Partain *et al.*⁷ had a hole concentration of order of 10^{20} cm^{-3} , which we estimate to correspond to about 0.2% Cu vacancies or $\text{Cu}_{1.996}\text{S}$. This may, in some small part, also contribute to the larger gaps found experimentally.

The gap is between mostly Cu d valence states and a mixture of Cu s and Cu p -like partial waves in the conduction band. One might expect that the d - p transitions are dominant because the d - s transitions are dipole forbidden. However, we should emphasize that this really means partial waves at the given energy rather than strict atomic Cu $4p$ orbitals. The conduction band really consists of itinerant free-electron-like electrons, or one can also think of them as Cu sp antibonding states with S sp . Compared to pure Cu, it is as if we have reduced the Cu d -band width by dispersing S atoms between them and moved up the free-electron-like Cu sp electrons slightly by their interaction with the S atoms. This is what leads to a band gap in the spectrum, compared to a Cu d band overlapping the free conduction electrons in metallic Cu. The conduction electrons in Cu_2S are thus rather free electrons with a fairly low effective mass, of about $0.3m_e$ as we estimated earlier. The holes, however, correspond to Cu d bands and have a rather high mass, in particular, in cubic material. This is important for the mobility in the materials and relevant to their intended uses as solar cell material.

We find somewhat lower gaps in cubic than in hexagonal modifications, but it is presently not clear if this is borne out by experiment because all experimental data on the gaps appear to correspond to hexagonal material. Nonetheless, it is perhaps worth pointing out that this is the usual situation for semiconductors which can exist both in wurtzite (hexagonal) and zinc-blende (cubic) forms. These also usually show a slightly lower gap in the cubic form.

VI. CONCLUSIONS

The main focus of this paper is the electronic band structure of Cu_{2-x}S . Large cell models for the hexagonal and cubic phase were constructed using a weighted random number algorithm that reproduces the statistical distribution of Cu atoms over the various Wyckoff sites in good agreement with experimental x-ray diffraction results. The structural models obtained show that in all phases, there are mixed Cu-S layers along close-packed planes with additional Cu atoms in between these layers. The band structure and density of states were calculated for the simple antiferroite structure as well as for the above model structures and the reported monoclinic

structure, which can be considered as having a nearly hexagonal structure. Models with slightly reduced Cu concentration, $0 < x < 0.2$, were also constructed and their electronic structure calculated.

Based on a comparison of the band structures of the simple antifluorite structure in LDA and in the QSGW method, and an analysis of the atomic orbital character of the bands, we added a simple correction to LDA by shifting up the Cu s derived bands. Although the antifluorite structure was found to remain metallic even after this correction to LDA, this is caused mainly by the degeneracy of the Cu d VBM due to the high symmetry of this structure. Breaking of this symmetry leads to the opening of a gap even in LDA, and this gap is then slightly increased by the Cu s shift. The band gaps of the larger and more realistic Cu_2S models increase from the cubic (0.4 eV) to the hexagonal (0.5 eV) to the monoclinic (0.6 eV) phase, but all gaps are significantly lower than the experimental values of about 1.1–1.2 eV found for the hexagonal structure. This probably indicates that our Cu s shift is not fully capturing the quasiparticle self-energy correction that would be obtained in a QSGW calculation. This is not too surprising because it is after all a very simplified correction. We also estimate from calculations of two slightly different structures with the same statistical distribution that the error bar on the gap arising from the structural uncertainty is at most 0.1 eV.

We find that the minimum band gap is direct in both the hexagonal and closely related monoclinic structure supercells. In reality, the distinction between direct and indirect band gaps for this material is difficult to make because of the disordered nature of the Cu distribution over different Wyckoff sites. This disorder implies that the electronic structure in Cu_2S has some similarities with that of an amorphous material, rather than a fully crystalline material. It should be kept in mind that band structures correspond to periodic boundary condition models but remain just representative models, not fully capturing the full complexity of the disordered state of these materials. The essentially direct nature of the gap is actually consistent with the fact that experimental data show absorption coefficients of order of 10^{-4} cm^{-1} , a few 0.1 eV above the gap even after intraband absorption is subtracted. This is 2 orders of magnitude higher than typical for an indirect band gap absorption. The typical experimental procedure of fitting a straight line in a plot of $\sqrt{\alpha}$ as function of photon energy to determine a minimum indirect gap is not reliable here because of the necessity to subtract a significant

free-carrier absorption and the fact that the band gaps can be expected to have an exponential tail due the almost amorphous nature of the Cu-atom distribution.

The experimental data found evidence for a second onset at about 0.5 eV above the minimum. This is consistent with an increase in density of states in the conduction band in our models at this energy, rather than the presence of transitions from a deeper valence band as previously suggested by experimentalists.

Reducing the Cu concentration of the samples is found to increase the optical absorption coefficient in two ways: (1) the Cu d band is slightly narrower, thus increasing the gap directly, and (2) the Fermi energy moves below the VBM, creating a degenerate hole doped system, which reduces the lowest possible optical transitions by the Moss-Burstein effect. For $0.06 < x < 0.2$, doping concentrations were found to be of order of $(0.8\text{--}2.4) \times 10^{21} \text{ holes/cm}^3$ and the Fermi level moved about 0.2–0.4 eV below the VBM. The trend agrees with the experimental trend of an increasing gap with decreasing Cu concentration. The gap is essentially between Cu d -like valence states and Cu sp -like conduction states.

The total energies of the system at zero temperature were found to increase from monoclinic to hexagonal to cubic phase, and the suggestion was made that the different temperature stability ranges of the different phases occur because of differences in vibrational free energy contribution between the different phases.

We found that the creation of Cu vacancies in Cu_2S is actually favorable even when the system is assumed to be in thermodynamic equilibrium with bulk Cu. This shows that Cu_2S is intrinsically unstable toward the formation of Cu_{2-x}S . This instability can be expected to be even stronger in an oxidizing environment since this would lower the chemical potential of Cu.

ACKNOWLEDGMENTS

This work was funded by the Air Force Office of Scientific Research. Computations were carried out at the Ohio Supercomputing Center, the Cluster Ohio Rev. 3 cluster of the Department of Physics, and the ITS high-performance computational cluster at Case Western Reserve University. M.v.S. and T.K. were supported by the Office of Naval Research Contract No. N00014-02-1-1025. They are also indebted to the Ira A. Fulton High Performance Computing Initiative. Useful discussions with Clemens Burda are gratefully acknowledged.

*Present address: Department of Physics, University of Nebraska, Omaha, NE 68182-0266, USA.

¹J. A. Bragagnolo, Allen M. Barnett, J. E. Phillips, R. B. Hall, A. Rothwarf, and J. D. Meakin, *IEEE Trans. Electron Devices* **ED-27**, 645 (1980).

²A. L. Fahrenbruch and R. H. Bube, *Fundamentals of Solar Cells* (Academic, New York, 1983).

³D. C. Reynolds, *Phys. Rev.* **96**, 533 (1954).

⁴G. Lis, T. Schulmeyer, J. Brötz, A. Klein, and W. Jaegerman, *Thin Solid Films* **431-432**, 477 (2003).

⁵L. R. Schiozawa, F. Augustine, G. A. Sullivan, J. M. Smith III, and W. R. Cook, Jr., *Clevite Final Report No. ARL PR 75/4*, 1975 (unpublished).

⁶F. Pfisterer, *Thin Solid Films* **431-432**, 470 (2003).

⁷L. D. Partain, P. S. McLeod, J. A. Duisman, T. M. Peterson, D. E. Sawyer, and C. S. Dean, *J. Appl. Phys.* **54**, 6708 (1983).

- ⁸V. I. Klimov and V. A. Karavanskii, *Phys. Rev. B* **54**, 8087 (1996); V. Klimov, P. Haring Bolivar, H. Kurz, V. Karavanskii, V. Krasovskii, and Yu. Krkishko, *Appl. Phys. Lett.* **67**, 653 (1995).
- ⁹Y.-B. Lou, A. C. S. Samia, J. Cowen, K. Banger, X. Chen, H. Lee, and C. Burda, *Phys. Chem. Chem. Phys.* **5**, 1091 (2003).
- ¹⁰Y. Lou, X. B. Cheng, A. C. Samia, and C. Burda, *J. Phys. Chem. B* **107**, 12431 (2003).
- ¹¹Y. B. Lou, M. Yin, S. O'Brien, and C. Burda, *J. Electrochem. Soc.* **152**, G427 (2005).
- ¹²L. Reijnen, B. Meester, A. Goossens, and J. Schoonman, *Chem. Vap. Deposition* **9**, 15 (2003).
- ¹³L. Reijnen, B. Feddes, A. M. Vredenberg, J. Schoonman, and A. Goossens, *J. Phys. Chem. B* **108**, 9133 (2004).
- ¹⁴L. Reijnen, B. Meester, A. Goossens, and J. Schoonman, *Chem. Mater.* **17**, 4142 (2005).
- ¹⁵L. Reijnen, B. Meester, and J. Schoonman, *Mater. Sci. Eng., C* **19**, 311 (2002).
- ¹⁶B. J. Mulder, *Phys. Status Solidi A* **15**, 409 (1973); **13**, 79 (1972); **13**, 569 (1972).
- ¹⁷G. P. Sorokin, Yu. M. Papshev, and P. T. Oush, *Sov. Phys. Solid State* **7**, 1810 (1966).
- ¹⁸A. G. Rastogi and S. Salkalachen, *Thin Solid Films* **97**, 199 (1982).
- ¹⁹P. S. McLeod, L. D. Partain, D. E. Sawyer, and T. M. Peterson, *Appl. Phys. Lett.* **45**, 472 (1984).
- ²⁰R. W. Potter, *Econ. Geol.* **72**, 1524 (1977).
- ²¹B. J. Wuensch and M. J. Buerger, *Miner. Soc. Am. Special Paper* **1**, 164 (1963).
- ²²M. J. Buerger and B. J. Wuensch, *Science* **141**, 276 (1963).
- ²³H. T. Evans, Jr., *Z. Kristallogr.* **150**, 299 (1979).
- ²⁴N. Morimoto and G. Kullerud, *Am. Mineral.* **48**, 110 (1963).
- ²⁵G. Will, E. Hinze, A. Rahman, and M. AbdelRahman, *Eur. J. Mineral.* **14**, 591 (2002).
- ²⁶R. Sadanaga, M. Ohmasa, and N. Morimoto, *Mineral. J.* **4**, 275 (1965).
- ²⁷S. Djurlle, *Acta Chem. Scand.* (1947-1973) **12**, 1415 (1958).
- ²⁸H. J. Gotsis, A. C. Barnes, and P. Strange, *J. Phys.: Condens. Matter* **4**, 10461 (1992).
- ²⁹E. Hiraehara, *J. Phys. Soc. Jpn.* **6**, 422 (1951); **6**, 428 (1951).
- ³⁰T. Kotani and M. van Schilfgaarde, *Solid State Commun.* **121**, 461 (2002).
- ³¹S. V. Faleev, M. van Schilfgaarde, and T. Kotani, *Phys. Rev. Lett.* **93**, 126406 (2004).
- ³²M. van Schilfgaarde, T. Kotani, and S. V. Faleev, *Phys. Rev. Lett.* **96**, 226402 (2006).
- ³³M. van Schilfgaarde, T. Kotani, and S. V. Faleev, *Phys. Rev. B* **74**, 245125 (2006).
- ³⁴T. Kotani, M. van Schilfgaarde, and S. Faleev, *Phys. Rev. B* **76**, 165106 (2007).
- ³⁵P. Hohenberg and W. Kohn, *Phys. Rev.* **136**, B864 (1964); W. Kohn and L. J. Sham, *ibid.* **140**, A1133 (1965).
- ³⁶L. Hedin and B. I. Lundqvist, *J. Phys. C* **4**, 2064 (1971).
- ³⁷M. Methfessel, M. van Schilfgaarde, and R. A. Casali, in *Electronic Structure and Physical Properties of Solids: The uses of the LMTO Method*, edited by Hugues Dreyssé, Springer Lecture Notes (Springer, Berlin, 2000), pp. 114–147.
- ³⁸E. Bott, M. Methfessel, W. Krabs, and P. C. Schmidt, *J. Math. Phys.* **39**, 3393 (1998).
- ³⁹L. Hedin, *Phys. Rev.* **139**, A796 (1965); L. Hedin and S. Lundqvist, in *Solid State Physics: Advances in Research and Applications*, edited by F. Seitz, D. Turnbull, and H. Ehrenreich (Academic, New York, 1969), Vol. 23, p. 1.
- ⁴⁰F. Aryasetiawan and O. Gunnarsson, *Phys. Rev. B* **49**, 16214 (1994).
- ⁴¹J. Ghijsen, L. H. Tjeng, J. van Elp, H. Eskes, J. Westerink, G. A. Sawatzky, and M. T. Czyzyk, *Phys. Rev. B* **38**, 11322 (1988).
- ⁴²S. F. Lin, W. E. Spicer, and R. S. Bauer, *Phys. Rev. B* **14**, 4551 (1976).
- ⁴³A. Kokalj, *Comput. Mater. Sci.* **28**, 155 (2003); code available from <http://www.xcrysden.org/>
- ⁴⁴T. S. Moss, *Proc. Phys. Soc. London, Sect. B* **67**, 775 (1954).
- ⁴⁵L. Burstein, *Phys. Rev.* **93**, 632 (1954).
- ⁴⁶C. Persson and A. Zunger, *Phys. Rev. Lett.* **91**, 266401 (2003).
- ⁴⁷P. Y. Yu and M. Cardona, *Fundamentals of Semiconductors* (Springer, Berlin, 1999), Chap. 6.